Applied Surface Science 480 (2019) 419–426

Contents lists available at ScienceDirect

Applied Surface Science

journal homepage: www.elsevier.com/locate/apsusc

Full length article

Mass transport in the PdCu phase structures during hydrogen adsorption and absorption studied by XPS under hydrogen atmosphere

Jiayi Tang[a,b], Susumu Yamamoto[a], Takanori Koitaya[c], Akitaka Yoshigoe[d], Takuma Tokunaga[a], Kozo Mukai[a], Iwao Matsuda[a,*], Jun Yoshinobu[a,*]

[a] The Institute for Solid State Physics, The University of Tokyo, 5-1-5, Kashiwanoha, Kashiwa, Chiba 277-8581, Japan
[b] Graduate School of Engineering, University of Hyogo, 2167, Shosha, Himeji, Hyogo 671-2280, Japan
[c] Department of Materials Molecular Science, Institute for Molecular Science, 38 Nishigo-Naka, Myodaiji, Okazaki 444-8585, Japan
[d] Materials Sciences Research Center, Japan Atomic Energy Agency, 1-1-1, Kouto, Sayo, Hyogo 679-5148, Japan

ARTICLE INFO

Keywords:
PdCu alloy
Hydrogen
Adsorption
Absorption
Ambient-pressure X-ray photoelectron spectroscopy

ABSTRACT

We investigated mass transports during hydrogen adsorption and absorption processes of PdCu alloys that has advantages of higher hydrogen diffusivity and economically lower-cost than the other Pd-alloys. The research was made with a comparison of the well-known ordered phase of the bcc structure (the B2 phase) and a mixed phase of the fcc and B2 structures. *In-situ* ultrahigh vacuum X-ray photoelectron spectroscopy (UHV-XPS) and ambient pressure X-ray photoelectron spectroscopy (AP-XPS) using synchrotron radiation were carried out to trace the chemical states of the Pd and Cu atoms as a function of temperatures. It is newly elucidated that the initial adsorption and absorption processes were similar in the two phases, but a hydrogen diffusion rate to the bulk was apparently higher in the ordered phase than in the mixed one. We found the dynamics of the Pd and Cu atoms during the hydrogen adsorption/absorption processes largely depends on temperature. In the hydrogen atmosphere, the Pd atoms segregate at the surface below 373 K and Cu atoms segregate at the surface above 373 K, showing a reversal behavior. The present results agree well with the previous theoretical calculations and, thus, provide appropriate inputs toward developments of the industrial hydrogen permeation materials.

1. Introduction

Pd-based alloys have recently attracted much interests of researchers as the hydrogen permeation materials that possess the higher hydrogen permeability and suppress the hydrogen embrittlement compared to elementary substance of Pd [1–7]. PdCu alloys, especially so-called "$PdCu_{40}$ alloy", has relatively higher hydrogen diffusivity than those of the other Pd-alloys (PdAg, PdAu, PdRh, *etc.*), improving the permeability efficiency, and high contents of Cu benefits economically by reducing material costs and by eliminating usage of rare metals. Moreover, Pd-Cu-H exhibits much smaller volume expansion and withstands thermal cycling in hydrogen permeation better, for example, than with PdAg [8].

Despite these advantages of PdCu alloys in the application fields, it leaves further improvements in microscopic aspects. For instance, hydrogen solubility of the face-centered cubic (fcc) structure of a PdCu alloy is approximately one order of magnitude higher than that of body-centered cubic (bcc) structure [9,10]. Many theoretical efforts, however, have resulted in proposing different performance in the hydrogen diffusivity and solubility with phase structures [11–15]. Further experimental evidence has been needed to settle this issue.

The hydrogen permeation generally follows the solution-diffusion mechanism, including 5 steps: (1) dissociative adsorption of H atoms on the surface, (2) dissolution of H atoms into the bulk, (3) diffusion of H atoms through the internal bulk, (4) association of H atoms on the surface on the opposite sides, (5) desorption as H_2 molecules from the surface. The step (3) has been accepted as the rate-limiting process of hydrogen permeability according to the Sievert's law [16,17], and thus it has been improved by reducing the membrane thickness to sub-μm. Now, the steps, (1) and (2), have become more significant to raise the permeation rate.

In the present research, we traced Pd and Cu atoms during hydrogen adsorption and absorption processes that are elemental in the steps (1) and (2) by the individual core-level photoelectron spectroscopies under the hydrogen atmosphere. The experiments were carried out with PdCu alloys with an ordered phase of the bcc structure (the B2 phase) and a mixed phase of the fcc and B2 structures to examine a microscopic role of the phase structure. Compared to the mixed phase, a hydrogen

* Corresponding authors.
E-mail addresses: imatsuda@issp.u-tokyo.ac.jp (I. Matsuda), junyoshi@issp.u-tokyo.ac.jp (J. Yoshinobu).

https://doi.org/10.1016/j.apsusc.2019.02.180
Received 31 October 2018; Received in revised form 18 February 2019; Accepted 19 February 2019
Available online 20 February 2019
0169-4332/

diffusion rate in the bulk was apparently higher in the ordered phase. On the other hand, the dynamical behaviors of the Pd and Cu atoms interaction with hydrogen in the two phases were basically similar to each other and they were found to depend much on temperature. In the hydrogen atmosphere, surface segregation proceeds with Pd atoms below 373 K, while, inversely, with Cu atoms above 373 K. These results provide significant information in designing and in fabricating the optimized PdCu alloys for the hydrogen permeability [18].

2. Experimental

2.1. Sample preparation

Samples of the $PdCu_{40}$ polycrystalline alloy (ϕ12.4 mm, d = 0.1 mm thickness) were supplied from Tanaka Kikinzoku Kogyo K.K. The bulk composition of as-received sample is nominally 60 wt% Pd and 40 wt% Cu (atomic ratio: 47.25% Pd, 52.75% Cu). Prior to the experiment, an ordered bcc phase (B2 phase) of the PdCu crystal was prepared by annealing at 673 K for 1 h. This process induces the phase transformation from the unstable fcc phase to the stable B2 phase. In order to obtain a fcc/B2 mixed phase structure, the B2-phased PdCu alloy was further annealed at 1000 K for 10 min by three cycles. The phase structures of the PdCu alloys were determined by X-ray diffraction measurements using a powder X-ray diffractometer (PANalytical X'PERT-Pro, Cu Kα radiation, λ = 1.5405 Å). Fig. 1(a) and (b) show the XRD patterns of the B2- and fcc/B2-phased PdCu alloys, respectively. It was observed that the PdCu alloy was a fully ordered B2 structure because there were only B2 peaks exist in the XRD pattern in Fig. 1(a). The PdCu alloy was a mixture phase of fcc and B2 because there were both fcc and B2 peaks in the XRD pattern as shown in Fig. 1(b). The clean surfaces of PdCu alloys were prepared by cycles of the Ar^+ ion sputtering at 1 keV(UHV-XPS) and 0.5 keV(AP-XPS) for 15 min and annealing at 673 K for 2 min. The clean surfaces were checked by C 1s and O 1s XPS spectra.

2.2. UHV-XPS

Ultrahigh vacuum XPS measurements were conducted using SUREAC2000 [19,20] at the soft X-ray beam line BL23SU [21] at SPring-8, Japan. The photoelectron spectra were measured using a hemispherical electron analyzer (EA125-5MCD, Omicron Nanotechnology GmbH). The circularly polarization X-ray was used in the UHV-XPS measurements, the incident and emission angles were 0° and 53° from the surface normal, respectively. Pure H_2 gas (> 99.99999%) exposure was carried out at 3.8×10^{-8} Torr under the base pressure of $< 2 \times 10^{-10}$ Torr at 300 K; subsequently, the sample temperature was raised in a stepwise manner up to 673 K. The Pd 3d and Cu 2p core-level spectra were recorded at the photon energies of 680 eV and 1100 eV, respectively.

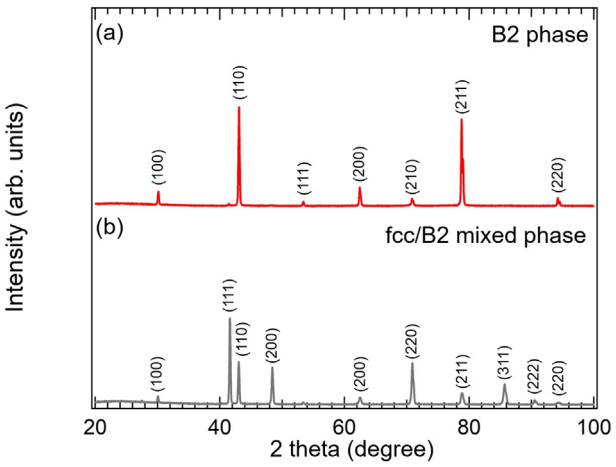

Fig. 1. XRD patterns of (a) B2 and (b) fcc/B2 mixed phased PdCu alloys in air.

2.3. AP-XPS

Ambient pressure XPS measurements were held at BL07LSU at SPring-8, Japan [22]. The horizontal linear polarized X-ray beam was used for the measurement. The incident and emission angles were 68° and 0°, respectively. The high-pressure pure H_2 gas (> 99.99999%) was introduced into an ambient-pressure gas cell under the base pressure below 5×10^{-10} Torr. During hydrogen exposure at 1.5 Torr, the sample temperature was raised from 300 K to 573 K. The Pd 3d and Cu 2p core-level spectra were measured at the photon energies of 680 eV and 1100 eV, respectively. The probing depths (3λ) are calculated to be ~2.03 nm for the kinetic energy of Pd 3d E_k(Pd 3d) at 345 eV and ~1.48 nm for E_k(Cu 2p) at 168 eV. Binding energies (BE's) of the measured spectra were calibrated by the Fermi energy. All the spectra were normalized by taking the average count of the background photoelectron at the low BE side. The peak position was determined in individual spectrum by curve-fitting using a Vogit function with the Shirley-type background.

3. Results and discussion

3.1. Hydrogen-adsorption process studied using UHV-XPS

The hydrogen adsorption processes on surfaces of the PdCu alloys (B2 and fcc/B2 phase) were studied by measuring *in situ* the high-resolution Pd $3d_{5/2}$ and Cu $2p_{3/2}$ core-level spectra during the hydrogen exposure at 3.8×10^{-8} Torr at 300–673 K. Fig. 2(a)–(f) show the evolution of the Pd $3d_{5/2}$ spectra under hydrogen pressure at 3.8×10^{-8} Torr on the B2 phase. The Pd $3d_{5/2}$ spectra on the clean surface and after the H_2 exposure are fit well with two components, one is located at the BE of 335.21 ± 0.02 eV and the other is at 335.82 ± 0.02 eV. The component located at the lower BE is assigned to the bulk Pd component, while the one located at the higher BE is assigned to the surface Pd component. This assignment is based on sensitivity of the lower BE component with the gas exposure, as described below, and also on the core-level shifts of Pd $3d_{5/2}$ spectra taken on the other Pd alloy of PdAg [23,24], in which the surface Pd component on the clean surface shifts to higher BE (+0.34 eV) with respect to the bulk component in the previous works [23,24]. The Pd $3d_{5/2}$ spectra taken on the fcc/B2 structure under the same conditions are depicted in Fig. 2(g)–(l). Similarly, two components (bulk and surface Pd) are observed on the fcc/B2 structure, whose BEs are 335.23 ± 0.03 eV (bulk Pd) and 335.82 ± 0.03 eV (surface Pd). Temperature dependence of Pd $3d_{5/2}$ on both the B2 and fcc/B2 phases show that surface Pd components gradually reduces with temperature above 473 K.

The Cu $2p_{3/2}$ region of XPS spectra taken on the clean surface and after the hydrogen exposure at 3.8×10^{-8} Torr at 300–673 K on the B2 and fcc/B2 phase surfaces are shown in Fig. 3. All the Cu $2p_{3/2}$ spectra are fit well with one component, whose BE is 932.07 ± 0.02 eV and 932.02 ± 0.02 eV on the B2 and fcc/B2 structures, respectively. The observed single component of the Cu $2p_{3/2}$ level may be assigned to the Cu atoms bonded with neighboring Cu or Pd atoms, notated as Cu-M (M: Cu, Pd). Energy positions of the Cu 2p photoelectrons are rather insensitive to the chemical environments [25]. Temperature dependence of Cu $2p_{3/2}$ spectra taken on B2 and fcc/B2 phases showed no obvious change during the H_2 exposure.

Fig. 4(a) and (b) summarize the intensity variations of surface and bulk Pd components in the Pd $3d_{5/2}$ spectra, observed on the clean surface and during the hydrogen adsorption at 300–673 K for the B2- and fcc/B2-phased PdCu alloys, respectively. The intensity of the surface Pd component was enhanced with increasing temperature during

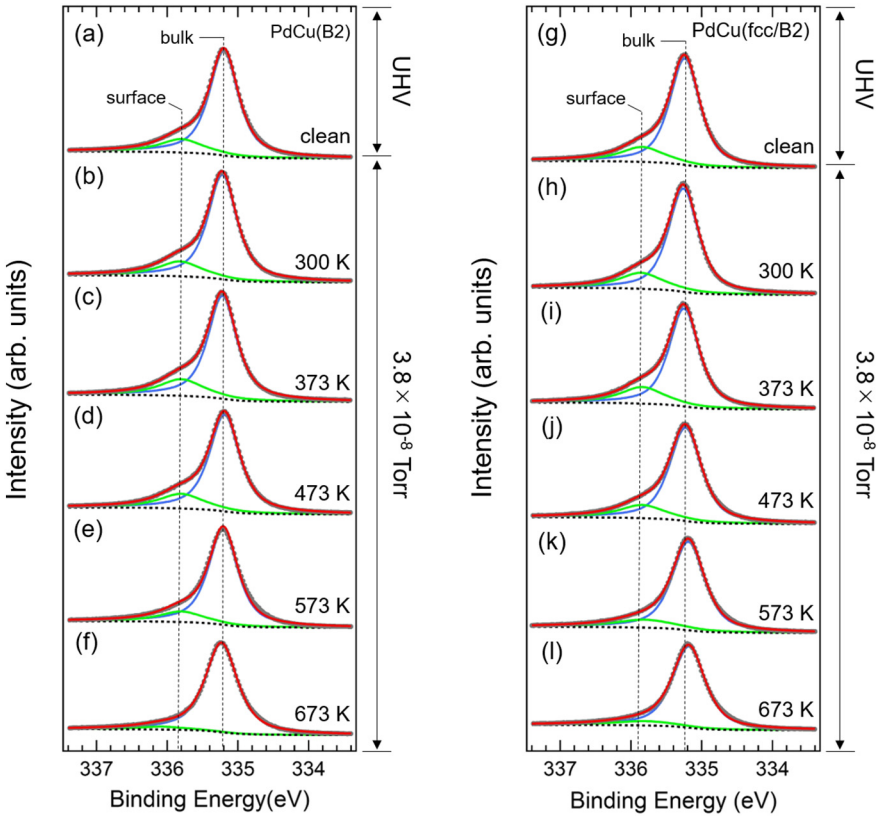

Fig. 2. Pd $3d_{5/2}$ spectra taken on (a) clean PdCu(B2) surface, and during H_2 exposure at 3.8×10^{-8} Torr at (b) 300 K, (c) 373 K, (d) 473 K, (e) 573 K, (f) 673 K on PdCu (B2) alloy. Pd $3d_{5/2}$ spectra taken on (g) clean PdCu(fcc/B2) surface, and during H_2 exposure at 3.8×10^{-8} Torr at (h) 300 K, (i) 373 K, (j) 473 K, (k) 573 K, (l) 673 K on PdCu(fcc/B2) alloy. The photon energy was set at 680 eV. Surface and bulk Pd components are shown with green and blue solid lines, respectively.

H_2 exposure at 300–373 K on both B2 and fcc/B2 phases. Conversely, the intensity of the bulk Pd component was reduced slightly on the B2 phase but significantly on the fcc/B2 phase. These results indicate enhancement of the surface Pd atoms and the reduction of the bulk Pd atoms, which corresponds to the Pd surface segregation. It is noted that the reduction was observed much significant for the fcc/B2 phase than for the B2 phase. This may be due to probing depth 3λ of ~2.03 nm that covers the different number of layers between the fcc/B2 phase (6

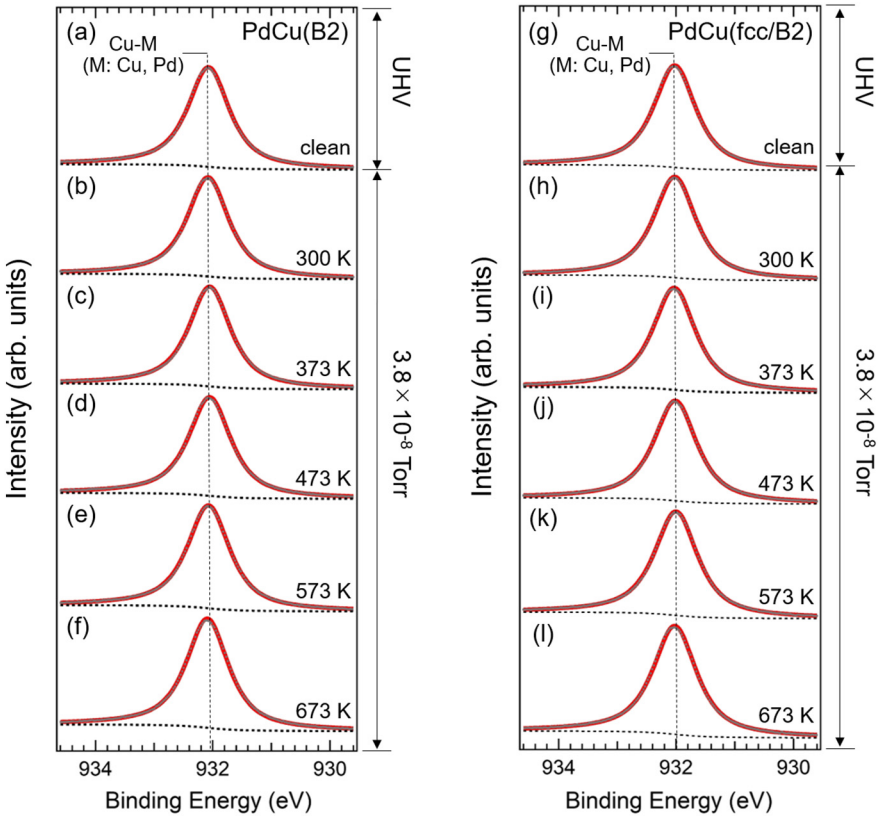

Fig. 3. Cu $2p_{3/2}$ spectra taken on (a) clean surface, and during H_2 exposure at 3.8×10^{-8} Torr at (b) 300 K, (c) 373 K, (d) 473 K, (e) 573 K, (f) 673 K on PdCu(B2) alloy. Cu $2p_{3/2}$ spectra taken on (g) clean surface, and during H_2 exposure at 3.8×10^{-8} Torr at (h) 300 K, (i) 373 K, (j) 473 K, (k) 573 K, (l) 673 K on PdCu(fcc/B2) alloy. The photon energy was set at 1100 eV.

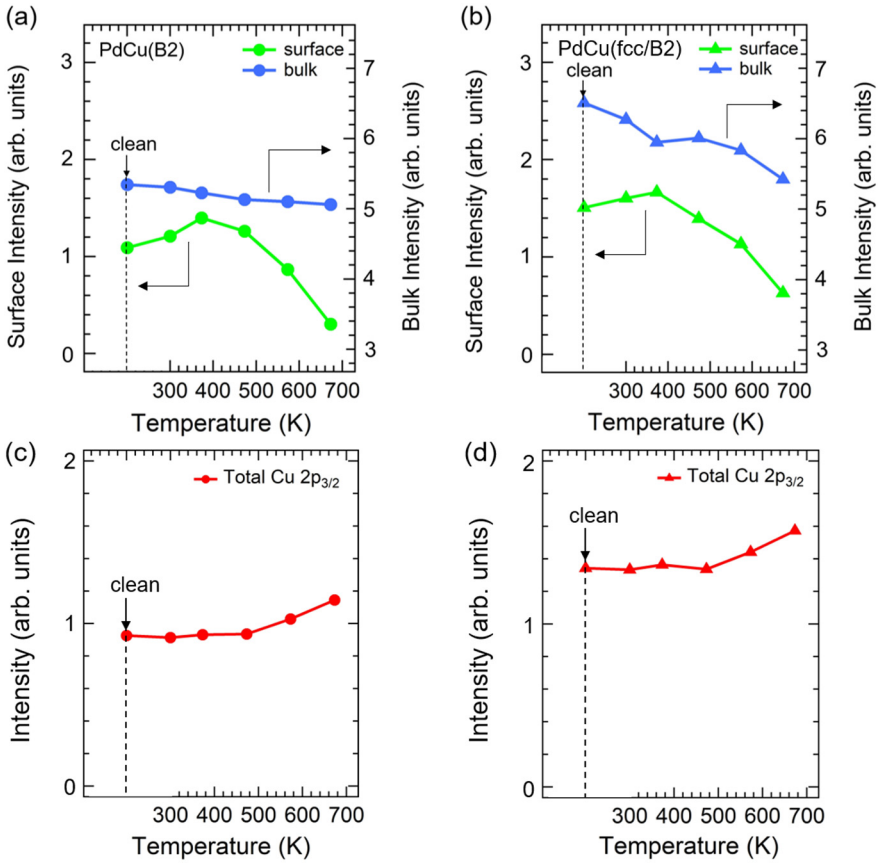

Fig. 4. Temperature dependences of intensities of surface (green) and bulk (blue) Pd components in the Pd $3d_{5/2}$ spectra obtained on the clean surface and during H_2 exposure at 3.8×10^{-8} Torr at 300–673 K on (a) B2 and (b) fcc/B2 phased PdCu alloys. Temperature dependences of the total intensities for Cu $2p_{5/2}$ spectra on the clean surface and during H_2 exposure at 3.8×10^{-8} Torr at 300–673 K on (c) B2 and (d) fcc/B2 phased PdCu alloys.

layers) and the B2 phase (7 layers).

In the temperature region of 373–673 K, on the other hand, the surface Pd atom drastically decreased and the bulk Pd atom slightly decreased with temperature on both the B2 and fcc/B2 phases. The result corresponds to the Cu transfer from the bulk to the surface of the PdCu(B2) and PdCu(fcc/B2) alloys, which are in good agreement with the significant enhancement of the total intensities of Cu $2p_{3/2}$ spectra with the temperature above 473 K, as shown in Fig. 4(c) and (d). The previous studies of the PdCu-H system also demonstrated a significant Cu surface segregation on the topmost layer, however, the near-surface region became Cu-depleted by annealing at 900 K in UHV [26,27].

Table 1 lists the intensity ratios of Pd $3d_{5/2}$ and Cu $2p_{3/2}$ spectra (I(Pd $3d_{5/2}$)/I(Cu $2p_{3/2}$)) on the clean surface and after H_2 exposure at 300–673 K on the B2 and fcc/B2 phases. We found that I(Pd $3d_{5/2}$)/I(Cu $2p_{3/2}$) was almost constant at 300–373 K, while it decreased at 373–673 K for the both two phases. It indicates that there is no composition change at 300–373 K, however, an enhancement of Cu content proceeds at 373–673 K in the near-surface region.

From the above results, evolutions of the alloy composition during hydrogen absorption can be divided into two temperature regions. At 300–373 K, Pd atoms in the near-surface region segregate to the topmost layer, in the meantime, Cu atoms on the topmost layer diffuse into the near-surface region, as shown in Fig. 5(a). At 373–673 K, Cu atoms segregate to both the topmost layer and near-surface region from the bulk as shown in Fig. 5(b). The hydrogen molecule is initially dissociatively adsorbed on the surface at 300 K, and the hydrogen coverage θ_H is gradually reduced by raising the temperature, as the hydrogen desorption generally occurs at 280–370 K on PdCu alloy [28]. Therefore, the segregation behaviors are probably influenced by θ_H, where Pd segregation occurs at high θ_H and Cu segregation occurs at low θ_H. This strong θ_H dependence is mainly due to the thermodynamic stability of the Cu-rich surface at the low θ_H while the Pd-rich surface is more stable at the high θ_H [29]. These results agree well with the theoretical calculations that a segregation reversal from Cu segregation at low coverage to Pd segregation at high coverage that in the presence of adsorbed hydrogen [30]. In addition, there is no phase-structure dependence during the hydrogen adsorption, therefore the dissociative adsorption is not the rate-limiting process in the hydrogen permeation.

Table 1
The ratios of total intensities of Pd $3d_{5/2}$ and Cu $2p_{3/2}$ spectra ($I_{Pd\ 3d}/I_{Cu\ 2p}$) on the clean surface and during H_2 adsorption at 3.8×10^{-8} Torr at 300–673 K on B2 and fcc/B2 phased alloys.

T (K)	P (Torr)	PdCu(B2)	PdCu(fcc/B2)
Clean	UHV	0.67	0.68
300	3.8×10^{-8}	0.68	0.68
373		0.69	0.65
473		0.66	0.63
573		0.59	0.57
673		0.50	0.47

3.2. Hydrogen-absorption process studied using AP-XPS

Temperature dependence of hydrogen absorption process on the B2 and fcc/B2 phases was observed by measuring the Pd $3d_{5/2}$ and Cu $2p_{3/2}$ core-level photoemission spectra during the hydrogen exposure at 1.5 Torr at 300–573 K. The Pd $3d_{5/2}$ spectrum taken on the clean surface is compared with those taken after H_2 exposure at 1.5 Torr at 300–573 K on the B2 phase, as shown in Fig. 6(a)–(e). There are two components, the bulk and the surface Pd atoms at the clean surface, as shown in the Section 3.1. The bulk and surface Pd are located at BEs of 335.03 eV and 335.67 eV, respectively. After the H_2 exposure at 300 K, the Pd $3d_{5/2}$ spectra are fitted with the several components. In addition to the bulk Pd components, one component located at BE of 335.38 eV can be attributed to the Pd hydride (bulk Pd—H), which is similar to the

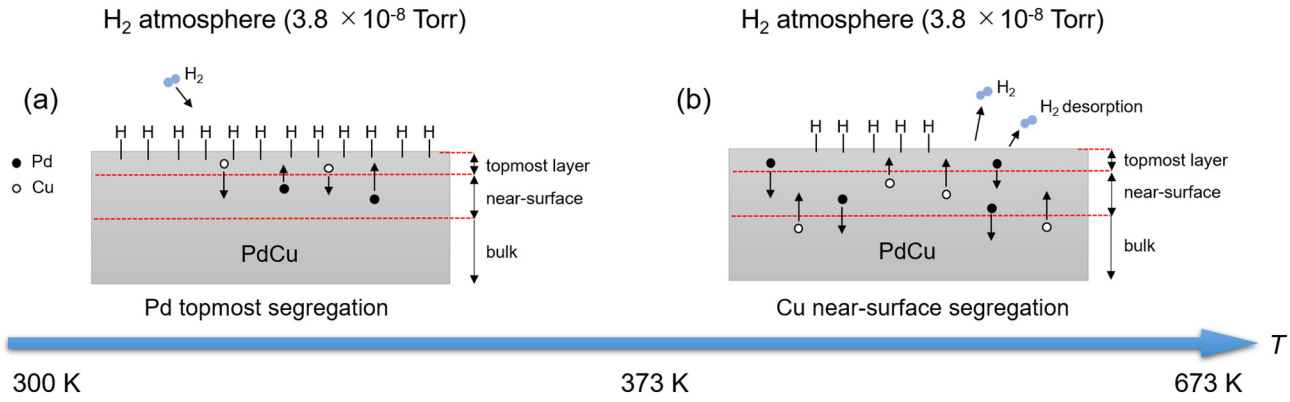

Fig. 5. The Schematic illustration of (a) Pd atoms segregation at 300–373 K, and (b) Cu atoms segregation at 373–673 K on the PdCu alloy during hydrogen exposure at 3.8 × 10^{-8} Torr.

assignment of the Pd hydride in the PdAg alloy [24]. A peak at BE of 335.63 eV probably originates from adsorption of the impurity CO molecules in the background [24]. As shown in Fig. 6(c), the component disappears at 373 K that may be due to the CO desorption. At 473–573 K, the Pd−H peak intensity increases significantly, indicating the enhancement of the Pd hydride formation. In the figures, one can also find that overall spectra, including the bulk Pd component and the Pd hydride component, shift to the higher BE side. The spectral feature may be associated with the changes in the chemical environment in the bulk PdCu alloy during the hydrogen absorption process. The similar observations can be found in the fcc/B2 phase in Fig. 6(f)–(j), where BEs of the surface, bulk Pd, and Pd hydride components are located at 335.77 eV, 335.13 eV and 335.5 eV, respectively. By comparing the B2 and fcc/B2 phases, it is intriguing to note that the Pd hydride formation in the B2 and fcc/B2 structures show the same behavior at 300–373 K, however, a larger amount of Pd hydrides are created in the B2 structure than in the fcc/B2 structure at 473–573 K.

Fig. 7(a)–(e) and (f)–(j) show the Cu $2p_{3/2}$ XPS spectra taken on the clean surface and after H_2 exposure at 1.5 Torr at 300–573 K in the B2 and fcc/B2 phases, respectively. The Cu $2p_{3/2}$ spectra taken on the clean surfaces of B2 and fcc/B2 structures are fit well by one component, whose BEs are 931.88 eV and 932.04 eV on B2 and fcc/B2 structures, respectively. It is assigned to the Cu-M (M: Cu, Pd), which is the similar with the Cu $2p_{3/2}$ result in the Section 3.1. After the hydrogen exposure at 1.5 Torr at 300 K, a new component appears at higher BE side with respect to the Cu-M component, whose BE shift is +0.36 eV in the B2 phase and + 0.38 eV in the fcc/B2 phase. This component originates from the Cu hydride (Cu−H), because the hydride always corresponds to the higher binding-energy side due to the electron deficiency of the Cu atoms caused by the Cu−H bond formation [31]. It is noted that the Cu-M component gradually shifts to the higher BE side, whereas the Cu−H component shifts to the lower BE side with the increase of temperature on both the B2 and fcc/B2 structures. It implies the changes of chemical environment during the hydrogen absorption at different temperature. The amount of Cu−H component is reduced by raising the temperature and the decrease rate of Cu−H component is higher in the B2 phase than fcc/B2 phase. Since the Pd−H component is enhanced more largely in the B2 phase than fcc/B2 phase by increasing

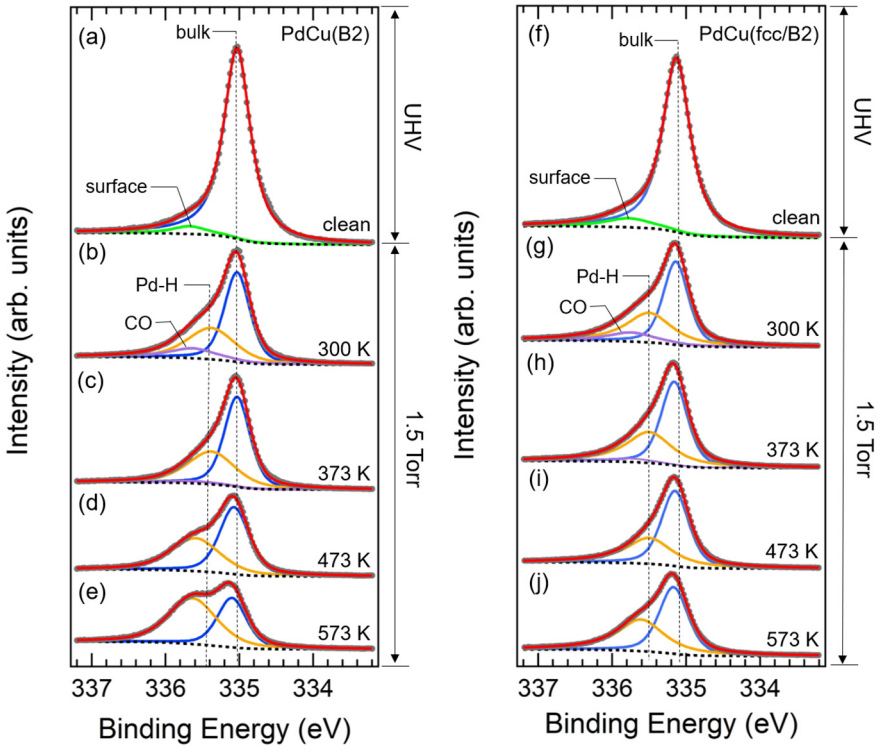

Fig. 6. Pd $3d_{5/2}$ spectra measured on (a) clean surface, and under H_2 exposure at 1.5 Torr at (b) 300 K, (c) 373 K, (d) 473 K, (e) 573 K on PdCu(B2) alloy. Pd $3d_{5/2}$ spectra measured on (f) clean surface, and under H_2 exposure at 1.5 Torr at (g) 300 K, (h) 373 K, (i) 473 K, (j) 573 K on PdCu(fcc/B2) alloy. The spectra were taken at photon energy of 680 eV. Surface Pd component, bulk Pd component, CO adsorption component and Pd−H component are presented with green, blue, purple, and yellow solid lines, respectively.

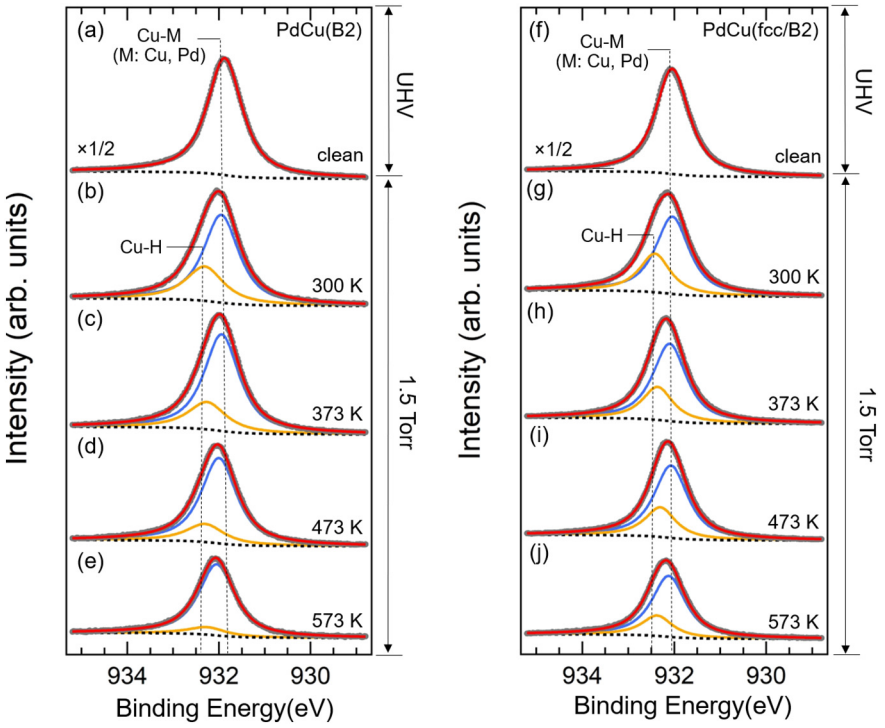

Fig. 7. Cu $2p_{3/2}$ spectra observed on (a) clean PdCu(B2) surface, and under H_2 exposure at 1.5 Torr at (b) 300 K, (c) 373 K, (d) 473 K, (e) 573 K on PdCu(B2) alloy. Cu $2p_{3/2}$ spectra observed on (f) clean PdCu(fcc/B2) surface, and under H_2 exposure at 1.5 Torr at (g) 300 K, (h) 373 K, (i) 473 K, (j) 573 K on PdCu(fcc/B2) alloy. The spectra were taken at photon energy of 1100 eV. Cu-M (M: Cu, Pd) components and Cu−H components are presented with blue and yellow solid lines, respectively.

temperature, the reactivity of the hydrogen absorption in the bulk is governed by the Pd sites.

The present research shows that the Pd−H formation of the B2 phase is reduced when the phase is mixed with the fcc phase, indicating the higher Pd−H reactivity in the B2 phase than in the fcc phase. On the other hand, it has been reported that the B2 (bcc) phase has the higher hydrogen diffusivity and the lower hydrogen solubility than the fcc phase [9,10,32]. A combination of these facts likely means that the rate-limiting factor in the hydrogen absorption in near-surface regions correspond to the hydrogen diffusivity rather than the hydrogen solubility.

The inverse temperature dependences of the Pd−H and Cu−H formations imply that the interstitial hydrogen occupied the different sites in the bulk at different temperature. Theoretical calculations have previously been carried out for PdCu alloys with 50% Pd and 50% Cu contents [13,14,33] and we recall the calculation results since the Pd/Cu composition ratio is similar to the present case, 47.25% Pd and 52.75% Cu. In the PdCu alloy, there are three possible interstitial H occupation sites, which are the octahedral sites (O1) and (O2), and the tetrahedral sites (T) [13,14,33]. Since binding energies (E_b) of the O sites are calculated, based on density functional theory, to be lower than those of T sites [34], the T sites are unfavorable and the O sites are the predominant trapping sites for hydrogen. Thus, we focus on the hydrogen occupations at the O sites. As shown in Fig. 8, the O1 site makes the hydrogen bonds with four Pd atoms and two Cu atoms (Pd rich), and the O2 site creates the hydrogen bonds with four Cu atoms and two Pd atoms (Cu rich) [14]. Moreover, E_b of the Pd-rich O1 site is estimated to be lower than that of Cu-rich O2 site on both the B2 and fcc structures [14], indicating O1 site is more energetically stable than O2 site.

In the present research, the temperature-dependent Pd $3d_{5/2}$ spectra and Cu $2p_{3/2}$ spectra show that the increase in a number of the Pd−H bonds is accompanied with the decrease in a number of the Cu−H bonds above 373 K. It indicates that occupations of the interstitial hydrogen sites depend on temperature. Considering these points, we can discuss that hydrogen atoms are initially trapped at O1 and O2 sites after H_2 exposure at 300 K. When the temperature is at 373–573 K, hydrogen atoms at the O2 sites diffuse to the energetically favorable O1 site throughout the PdCu alloy, and the diffusion rate is further enhanced at 573 K since the H diffusivity increases by three orders of magnitudes from 300 K to 500 K [33]. It can be inferred that the hydrogen atoms diffusion from O2 to O1 site behaves more active in the B2 phase than in the fcc/B2 phase due to the lower activation energy of the hydrogen diffusion through the bulk of B2 phase [14,35–38].

These results, after all, indicate that, in the near-surface region, diffusion process is the rate-limiting factor in hydrogen permeation and

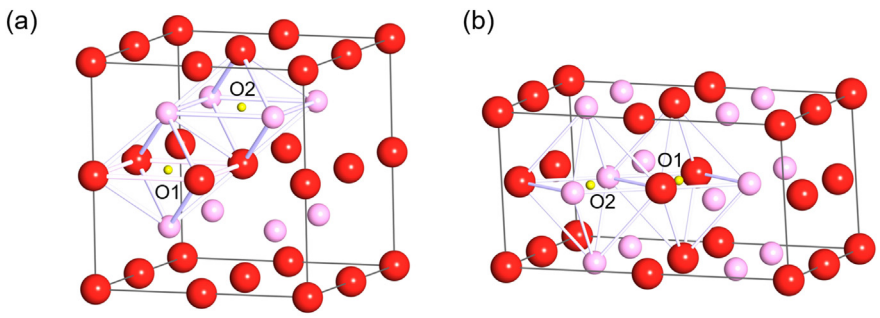

Fig. 8. Octahedral sites (O1 and O2) of hydrogen atom in the (a) B2 and (b) fcc phased PdCu alloy. The red and pink spheres represent Pd and Cu atoms, respectively. The small yellow balls stand for the interstitial sites.

the diffusion rate is higher in the B2 phase than the mixed fcc/B2 phase or the fcc phase. Our previous work on the PdAg-H system shows that no hydrogen absorption happens at 300–373 K and suddenly occurs above 473 K under the hydrogen atmosphere at 1.5 Torr [24]. It is further confirmed that the activation energy of hydrogen absorption in the PdCu alloy is lower than that in the PdAg alloy, especially in the low temperature region of 300–373 K. This can be understood by the higher hydrogen diffusivity of PdCu alloy than PdAg alloy [39], being consistent to the present discussion of the critical role of the hydrogen diffusion at the surface region, which further improve the permeability efficiency in the PdCu alloy.

4. Conclusions

We carried out the *in-situ* UHV-XPS and AP-XPS measurements to comparatively and systematically study the hydrogen interactions with the surface and bulk on the B2- and fcc/B2- phased PdCu alloys during the hydrogen adsorption and absorption processes. It is found that the behaviors of the hydrogen adsorption slightly depend on the phase structures. Interestingly, the reverse surface segregation in the surface and near-surface regions with the increase of temperature was newly observed, which was influenced by the hydrogen coverage on the surface. We observed the hydride formation at low temperature region of 300–373 K on the PdCu alloy, which is different from that on PdAg alloy [24]. The strong temperature and phase-structure dependences were found during the hydrogen absorption in the PdCu alloy. The hydride formation is significantly enhanced at 473 K, which corresponds to the hydrogen diffusion from the Cu-rich O2 site to the energetically favorable Pd-rich O1 site. Further, the activation energy of the hydrogen diffusion was found to be lower in the B2 phase than that in the fcc/B2 phase, which caused a larger enhancement of the hydride formation in the B2 phase. Our elucidation of hydrogen diffusion mechanisms on the different phase structures gives a new understanding of the hydrogen absorption process, which could be the critical point for the rate-limiting process in the hydrogen permeation through the PdCu alloy. In terms of perspectives, with the development of the high permeability efficiency membrane by reducing the thickness, more attentions should be paid on the interactions of hydrogen with the surface and near-surface region for well controlling the permeation process.

Acknowledgements

This study was supported by the Advanced-Catalytic-Transformation program for Carbon utilization (ACT-C) of the Japan Science and Technology Agency (JST, Grant No. JPMJCR12YU), JSPS Grant-in-Aid for Scientific Research on Innovative Area (“3D Active-Site Science”, Grant No. 17H05212; “Hydrogenomics”, Grant No. 18H05517), and JSPS Grant-in-Aid for Young Scientists (A) (No. 16H06027). The synchrotron-radiation UHV-XPS experiments were performed at SPring-8 BL23SU with the approval of the Japan Synchrotron Radiation Research Institute (Proposal Nos. 2017A3835, 2017A3801, 2017B3801). The AP-XPS measurement using synchrotron radiation were carried out at SPring-8 BL07LSU as joint research in the Synchrotron Radiation Research Organization and The Institute for Solid State Physics, The University of Tokyo (Proposal Nos. 2016B7401, 2017A7401, 2017B7401, 2018A7557). The PdCu alloy samples was supplied by Tanaka Kikinzoku Kogyo K. K. We gratefully acknowledge the help of Toyoto Sato (Tohoku Univ.) and Okkyun Seo (NIMS) in assisting with XRD measurements and analysis.

References

[1] Z. Ozturk, F. Sen, S. Sen, G. Gokagac, The preparation and characterization of nano-sized Pt–Pd/C catalysts and comparison of their superior catalytic activities for methanol and ethanol oxidation, J. Mater. Sci. 47 (2012) 8134–8144.
[2] H. Göksu, Y. Yıldız, B. Çelik, M. Yazıcı, B. Kılbaş, F. Şen, Highly efficient and monodisperse graphene oxide furnished Ru/Pd nanoparticles for the dehalogenation of aryl halides via ammonia borane, Chemistryselect 1 (2016) 953–958.
[3] B. Çelik, Y. Yıldız, H. Sert, E. Erken, Y. Koşkun, F. Şen, Monodispersed palladium–cobalt alloy nanoparticles assembled on poly(*N*-vinyl-pyrrolidone) (PVP) as a highly effective catalyst for dimethylamine borane (DMAB) dehydrocoupling, RSC Adv. 6 (2016) 24097–24102.
[4] B. Sen, B. Demirkan, A. Şavk, S.K. Gülbay, F. Şen, Trimetallic PdRuNi nanocomposites decorated on graphene oxide: a superior catalyst for the hydrogen evolution reaction, Int. J. Hydrog. Energy 43 (2018) 17984–17992.
[5] B. Sen, S. Kuzu, E. Demir, S. Akocak, F. Sen, Monodisperse palladium–nickel alloy nanoparticles assembled on graphene oxide with the high catalytic activity and reusability in the dehydrogenation of dimethylamine–borane, Int. J. Hydrog. Energy 42 (2017) 23276–23283.
[6] B. Sen, S. Kuzu, E. Demir, E. Yıldırır, F. Sen, Highly efficient catalytic dehydrogenation of dimethyl ammonia borane via monodisperse palladium–nickel alloy nanoparticles assembled on PEDOT, Int. J. Hydrog. Energy 42 (2017) 23307–23314.
[7] O. Seo, J. Kim, S. Hiroi, C. Song, L.S.R. Kumara, A. Tayal, Y. Chen, H. Kobayashi, H. Kitagawa, O. Sakata, Lattice constant, bond-orientational order, and solid solubility of PdPt bimetallic nanoparticles, Appl. Phys. Lett. 113 (2018) 071907.
[8] D.L. McKinley, Method for hydrogen separation and purification. U.S. Patent 3,439, 474, April 22, 1969.
[9] X. Zhang, W. Wang, J. Liu, S. Sheng, G. Xiong, W. Yang, Hydrogen transport through thin palladium-copper alloy composite membranes at low temperatures, Thin Solid Film 516 (2008) 1849–1856.
[10] W. Huang, S.M. Opalka, D. Wang, T.B. Flanagan, Thermodynamic modelling of the Cu-Pd-H system, CALPHAD 31 (2007) 315–329.
[11] J. Shu, B.P.A. Grandjean, A. Van Neste, S. Kaliaguine, Catalytic palladium-based membrane reactors: a review, Can. J. Chem. Eng. 69 (1991) 1036–1060.
[12] C. Decaux, R. Ngameni, D. Solas, S. Grigoriev, P. Millet, Time and frequency domain analysis of hydrogen permeation across PdCu metallic membranes for hydrogen purification, Int. J. Hydrog. Energy 35 (2010) 4883–4892.
[13] P. Kamakoti, D.S. Sholl, A comparison of hydrogen diffusivities in Pd and CuPd alloys using density functional theory, J. Membr. Sci. 225 (2003) 145–154.
[14] L.C. Liu, J.W. Wang, Y.H. He, H.R. Gong, Solubility, diffusivity, and permeability of hydrogen at PdCu phases, J. Membr. Sci. 542 (2017) 24–30.
[15] R.J. Westerwaal, E.A. Bouman, W.G. Haije, H. Schreuders, S. Dutta, M.Y. Wu, C. Boelsma, P. Ngene, S. Basak, B. Dam, The hydrogen permeability of Pd-Cu based thin film membranes in relation to their structure: a combinatorial approach, Int. J. Hydrog. Energy 40 (2015) 3932–3943.
[16] R.C. Hurlbert, J.O. Konecny, Diffusion of hydrogen through palladium, J. Chem. Phys. 34 (1961) 655–658.
[17] A. Caravella, G. Barbieri, E. Drioli, Modelling and simulation of hydrogen permeation through supported Pd-based membranes with a multicomponent approach, Chem. Eng. Sci. 63 (2008) 2149–2160.
[18] L. Yuan, A. Goldbach, H. Xu, Segregation and H_2 transport rate control in body-centered cubic PdCu membranes, J. Phys. Chem. B 111 (2007) 10952–10958.
[19] A. Yoshigoe, Y. Teraoka, Adsorption dynamics on Si(111)-7×7 surface induced by supersonic O_2 beam studied using real-time photoelectron spectroscopy, J. Phys. Chem. C 114 (2010) 22539–22545.
[20] A. Yoshigoe, Y. Teraoka, Synchrotron radiation photoelectron spectroscopy study on oxide evolution during oxidation of a Si(111)-7×7 surface at 300 K: comparison of thermal equilibrium gas and supersonic molecular beams for oxygen adsorption, J. Phys. Chem. C 118 (2014) 9436–9442.
[21] Y. Saitoh, Y. Fukuda, Y. Takeda, H. Yamagami, S. Takahashi, Y. Asano, T. Hara, K. Shirasawa, M. Takeuchi, T. Tanaka, H. Kitamura, Performance upgrade in the JAEA actinide science beamline BL23SU at SPring-8 with a new twin-helical undulator, J. Synchrotron Radiat. 19 (2012) 388–393.
[22] S. Yamamoto, Y. Senba, T. Tanaka, H. Ohashi, T. Hirono, H. Kimura, M. Fujisawa, J. Miyawaki, A. Harasawa, T. Seike, S. Takajashi, N. Nariyama, T. Matsushita, M. Takeuchi, T. Ohata, Y. Furukawa, K. Takeshita, S. Goto, Y. Harada, S. Shin, H. Kitamura, A. Kakizaki, M. Oshima, I. Matsuda, New soft X-ray beamline, BL07LSU at SPring-8, J. Synchrotron Rad. 21 (2014) 352–365.
[23] L.E. Walle, H. Gronbeck, V.R. Fernandes, S. Blomberg, M.H. Farstad, K. Schulte, J. Gustafson, J.N. Andersen, E. Lundgren, A. Borg, Surface composition of clean and oxidized $Pd_{75}Ag_{25}$(100) from photoelectron spectroscopy and density functional theory calculations, Surf. Sci. 606 (2012) 1777–1782.
[24] J. Tang, S. Yamamoto, T. Koitaya, Y. Yoshikura, K. Mukai, S. Yoshimoto, I. Matsuda, J. Yoshinobu, Hydrogen adsorption and absorption on a Pd-Ag alloy surface studied using in-situ X-ray photoelectron spectroscopy under ultrahigh vacuum and ambient pressure, Appl. Surf. Sci. 463 (2019) 1161–1167.
[25] M.V. Castegnaro, A. Gorgeski, B. Balke, M.C.M. Alves, J. Morais, Charge transfer effects on the chemical reactivity of Pd_xCu_{1-x} nanoalloys, Nanoscale 8 (2016) 641–647.
[26] F. Cheng, X. He, Z. Chen, Y. Huang, Kinetic Monte Carlo simulation of surface segregation in Pd-Cu alloys, J. Alloy. Compd. 648 (2015) 1090–1096.
[27] J.B. Miller, C. Matranga, A.J. Gellman, Surface segregation in a polycrystalline $Pd_{70}Cu_{30}$ alloy hydrogen purification membrane, Surf. Sci. 602 (2008) 375–382.
[28] M.S. Mousa, J. Loboda-Cackovic, J.H. Block, Thermal desorption spectroscopy analysis of oxygen from Pd-rich surfaces of PdCu(110) single crystal, Vacuum 48 (1997) 375–381.
[29] M. Tang, H. Li, W. Yuan, S. Zou, C. Sun, Y. Wang, First-principles study of the interactions of hydrogen with low-index surfaces of PdCu ordered alloy, Progress in Natural Science: Materials International 27 (2017) 709–713.
[30] B.C. Khanra, M. Menon, Role of adsorption on surface composition of Pd-Cu nanoparticles, Physica B 270 (1999) 307–312.

[31] I.L. Soroka, A. Shchukarev, M. Jonsson, N.V. Tarakina, P.A. Korzhavyi, Cuprous hydroxide in a solid form: does it exist? Dalton Trans. 42 (2013) 9585–9594.
[32] C. Zhao, A. Goldbach, H. Xu, Low-temperature stability of body-centered cubic PdCu membranes, J. Membr. Sci. 542 (2017) 60–67.
[33] P. Kamakoti, D.S. Sholl, Ab initio lattice-gas modeling of interstitial hydrogen diffusion in CuPd alloys, Phys. Rev. B 71 (2005) 014301.
[34] L. Semidey-Flecha, D.S. Sholl, Combining density functional theory and cluster expansion methods to predict H_2 permeance through Pd-based binary alloy membrane, J. Chem. Phys. 128 (2008) 144701.
[35] L. Yuan, A. Goldbach, H. Xu, Permeation hysteresis in PdCu membranes, J. Phys. Chem. B 112 (2008) 12692–12695.
[36] B.H. Guerreiro, M.H. Martin, L. Roué, D. Guay, Hydrogen permeability of PdCuAu membranes prepared from mechanically-alloyed powders, J. Membr. Sci. 509 (2016) 68–82.
[37] Y. Matsumura, A basic study of high-temperature hydrogen permeation through bcc Pd-Cu alloy foil, Sep. Purif. Technol. 138 (2014) 130–137.
[38] M.D. Dolan, Non-Pd BCC alloy membranes for industrial hydrogen separation, J. Membr. Sci. 362 (2010) 12–28.
[39] G. Alefeld, J. Völkl, Eds.; Topics in Applied Physics 28, Springer, Berlin, 1978, pp. 321–348.